CERN-INTC-2023-005 / INTC-P-650
11/01/2023

EUROPEAN ORGANIZATION FOR NUCLEAR RESEARCH

Proposal to the ISOLDE and Neutron Time-of-Flight Committee

Exploring the evolution of the $N = 126$ magic number with the masses of neutron-rich gold isotopes

January 11, 2023

V. Manea[1], K. Blaum[2], D. Lange[2], Yu. A. Litvinov[3], D. Lunney[1], M. Mougeot[4], S. Naimi[1], L. Nies[5,6], Ch. Schweiger[2], L. Schweikhard[6], F. Wienholtz[7], A. Andreyev[8,*]

[1] *Université Paris-Saclay, CNRS/IN2P3, IJCLab, 91405 Orsay, France*
[2] *Max-Planck-Institut für Kernphysik, Saupfercheckweg 1, 69117 Heidelberg, Germany*
[3] *GSI Helmholtzzentrum für Schwerionenforschung GmbH, Planckstraße 1, 64291 Darmstadt, Germany*
[4] *University of Jyväskylä, P.O. Box 35, FI-40014 University of Jyväskylä, Finland*
[5] *CERN, 1211 Geneva 23, Switzerland*
[6] *Universität Greifswald, Institut für Physik, 17487 Greifswald, Germany*
[7] *Institut für Kernphysik, Technische Universität Darmstadt, 64289 Darmstadt, Germany*
[8] *Department of Physics, University of York, York, YO10 5DD, United Kingdom*
[*] *For the IDS collaboration*

Spokesperson: V. Manea (vladimir.manea@ijclab.in2p3.fr)
Contact person: L. Nies (lukas.nies@cern.ch)

Abstract: We propose to measure the masses of the neutron-rich gold isotopes $^{204-206}$Au with the ISOLTRAP mass spectrometer, with the aim to improve the understanding of nuclear structure along the $N = 126$ magic number. The new masses would allow determining neutron separation energies and the empirical shell gap at $N = 126$, closer to the neutron dripline. The measurements would test the predictions of recent nuclear-structure models, constrain the monopole interaction and the quadrupole correlation energy and improve the predictions of separation energies and beta-decay Q-values. The new data would not only expand the study of shell evolution in exotic nuclei, but also improve the nuclear-physics input for modeling the r-process of nucleosynthesis.

Requested shifts: 17 shifts in 1 run.

Motivation

Magic numbers are the backbone of nuclear structure [1, 2] and the properties of magic or near-magic nuclei are essential for constraining nuclear-structure models. Of these properties, the ground-state binding energy is a quantity of fundamental importance, because it gives access to the empirical shell gap and to the (effective) single-particle energies (ESPE). The shell gap and the ESPEs are linked to the mean-field picture of the nucleus and their evolution is sensitive to the monopole interaction. In odd and odd-odd systems, binding energies are also sensitive to the energy of pairing correlations or to the residual proton-neutron interaction. In nuclei with two nucleons added or removed from a magic number, they also reflect the gain in binding by configuration mixing (typically through quadrupole correlations). These pieces of information are essential, together with other observables, for constructing a comprehensive picture of nuclear structure.

In this proposal, we aim to extend the knowledge of nuclear binding energies around the $N = 126$ magic number to the gold isotopic chain, by measuring the masses of $^{204-206}$Au. The new data would allow testing the large-scale shell model, such as the recent approach of [3], which has an excellent agreement to experimentally known binding energies. It would also confirm whether its description of the trends of two-neutron separation energies in the vicinity of the magic number is correct, which depends on the correct description of quadrupole correlations, as will be discussed below. By benchmarking the shell model, the proposed measurements would increase the reliability of its predictions towards the neutron dripline. This would not only improve the understanding of nuclear structure along the $N = 126$ magic number, but also the description of neutron separation energies and beta-decay Q-values of nuclei which cannot be produced in sufficient quantities. Both are involved in the calculation of input quantities for modeling the r-process of nucleosynthesis [4]. The occurrence of the third peak in the abundance of the r-process elements (around mass $A \approx 200$) is linked to the $N = 126$ magic number and the properties of nuclei in the region are essential for its description in reaction-network calculations. In these models, separation energies are used for calculating photo-dissociation rates via the detailed balance. Moreover, the beta-decay Q-values enter in the calculation of beta-decay rates [5]. Therefore, constraining the slope of the empirical shell gap below $Z = 82$ and the detailed shape of the mass surface around the $N = 126$ magic number also improves the calculations of the nuclear-physics input for the study of the r-process. In addition, ^{208}Pb has recently entered the reach of ab initio calculations [6]. This means that the new experimental data would motivate further developments of ab initio many-body methods and allow to test their description of the shell structure of heavy nuclei, a region where comparisons of experiment and ab-initio calculations are so far virtually nonexistent.

The study of $^{204-206}$Au would also mark the first laser ionization of gold isotopes across the $N = 126$ shell closure. This could set the stage for a later in-source laser spectroscopy experiment, aimed at determining the kink of charge radii across $N = 126$, continuing the previous studies performed at ISOLDE in the mercury isotopic chain [7].

Context

In the last decades the binding energies of many magic or near-magic nuclei have been determined with high precision and have allowed tracing the evolution of magic numbers with neutron-proton asymmetry. ISOLTRAP has contributed to several of these measurements [8, 9, 10, 11, 12, 13, 14]. In the light mass region, neutron magic numbers were found to strongly depend on proton number with the notable examples of the $N = 20$ and $N = 28$ [15, 16, 17] gaps vanishing with the removal of protons from the $Z = 20$ core and the $N = 32, 34$ [10, 18, 19] sub-shell gaps being increased around the calcium isotopic chain ($Z = 20$). The case of $N = 20$ is illustrated in fig. 1 which shows the *two-neutron* empirical shell gap (Δ_{2n}, in black), quantifying the drop in the two-neutron separation energy at the crossing of the magic neutron number. The vanishing of the magic number is seen through the significant reduction of Δ_{2n} towards $Z = 10$.

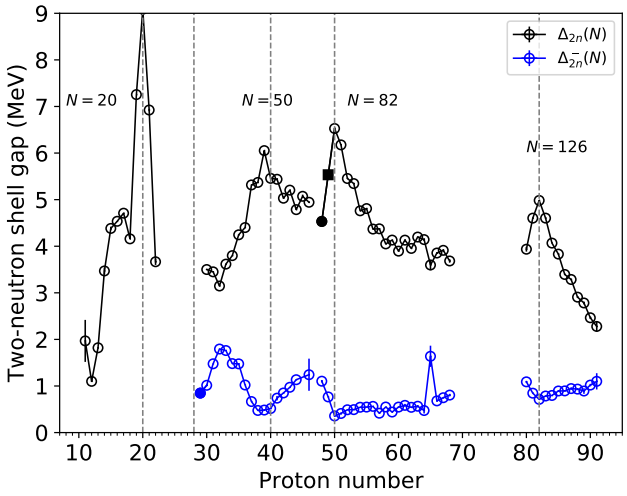

Figure 1: Experimental values from [20] (open circles), [12] (blue full circle), [14] (black full circle) and [21] (black square) of the two-neutron empirical shell gap in its normal (black) and shifted version (blue), called Δ_{2n} and Δ^{-}_{2n}, respectively, for some of the important magic neutron numbers. The values are presented as a function of proton number (see text for details).

For the higher neutron magic numbers ($N = 50, 82, 126$), the situation is less clear, as can be again seen in fig. 1. One observes a reduction with $\sim A^{-2/3}$ of the monopole interaction strength [1], which is considered the driving force of shell evolution. In the case of $N = 50$, it was shown that the shell gap is already reduced in ^{78}Ni to the point that low-lying intruder states are found [22], while theoretical studies predict an island of deformation developing once protons start to be removed from $Z = 28$ [23]. In the case of $N = 82$, the large gap at ^{132}Sn ($Z = 50$) [8] was recently shown to be significantly reduced by removing only two protons from $Z = 50$, which could very well continue towards $Z = 40$ [14]. As in the case of light nuclei, activating protons in new shells (by opening the $Z = 28$ or $Z = 50$ cores), can dramatically change the overall effect of the monopole Hamiltonian [1].

In the case of $N = 126$, the empirical shell gap is known to $Z = 80$, as shown in figs. 1 and 2. The upper left panel of fig. 2 shows the neutron binding energies below and above the $N = 126$ magic number, calculated as (minus) the neutron separation energies from the $N = 126$ and $N = 127$ isotones, respectively. The *one-neutron* empirical shell gap Δ_n shown in the lower left panel is (by definition) the difference between the two curves.

One can see that the gap is increasing towards $Z = 82$, making ^{208}Pb a robust doubly magic nucleus. Below $Z = 82$, the gap starts to be gradually reduced.

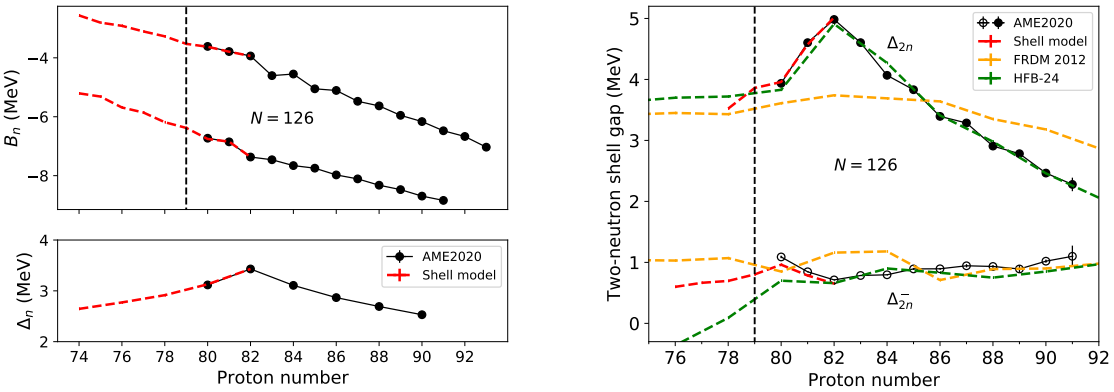

Figure 2: Left: Experimental [20] neutron binding energies around the $N = 126$ shell gap (top) and one-neutron empirical shell gap (bottom) as a function of proton number. Right: Two-neutron empirical shell gap as a function of proton number, in two variants, the regular Δ_{2n} (calculated for $N = 126$) and the shifted Δ^-_{2n} (calculated for $N = 124$). Theoretical values are also presented: the shell model of [3] (red), the finite-range droplet model of [24] (orange) and the Hartree-Fock-Bogoliubov mass model of [25] (green).

In fig. 2 the experimental data are compared to theoretical models, including the recent shell-model calculations of [3] (red). The model gives a very good description of the data and predicts that Δ_n will continue to decrease from ≈ 3.4 MeV in ^{208}Pb to about 2.7 MeV at $Z = 74$, which can be enough for low-lying intruder states to occur (as is the case for ^{78}Ni [26, 22]). The Δ_n value is however also affected by quadrupole correlations, which can be seen by the slightly non-linear trend. This effect is stronger in the case of the *two-neutron* empirical shell gap Δ_{2n} (right panel of fig. 2), because Δ_{2n} reflects the structure of nuclei with two valence neutrons (particles or holes). Its peak at the crossing of $Z = 82$ is more prominent than the one of Δ_n, which is known as the phenomenon of "mutually enhanced magicity" [27, 28]. This is because Δ_{2n} not only reflects the variation with proton number of the ESPEs, but also of the quadrupole correlation energy, minimized when crossing a proton magic number, as shown in [29].
A complementary effect is observed if the shell gap is computed two neutrons below the magic number (at $N_0 - 2$), as discussed in [12]. As shown in fig. 1 with blue symbols, the variation of this so-called shifted shell gap, called Δ^-_{2n}, is anti-correlated to Δ_{2n}, having a local minimum where the latter has a maximum. This behavior can again be explained by the variation with proton number of the quadrupole correlation energy [30]. In the right panel of fig. 2, the shifted shell gap is also plotted for the $N = 126$ magic number. One can notice that for existing experimental data the anti-correlation is confirmed and well described by the locally constrained model of [3]. For $Z < 80$, the behavior predicted by the model contradicts the expectation, because the shell model predicts the Δ^-_{2n} values to decrease, while the contrary would be expected. Global models such as the ones of [24] and [31] miss the details of Δ^-_{2n}, but predict an exceptionally flat Δ_{2n} for $Z < 80$.

Experimental setup

The measurements will be performed with the ISOLTRAP mass spectrometer [32, 33], which is presented in fig. 3. It consists of four ion traps used for beam preparation and measurement. The quasi-continuous ion beam provided by ISOLDE is cooled and bunched in a linear radio-frequency quadrupole (RFQ) [34]. Ion bunches are ejected from the RFQ and transferred to the multi-reflection time-of-flight mass spectrometer (MR-ToF MS) [33]. The MR-ToF MS can be used as a mass measurement apparatus. When the contamination level is high, it can alternatively be used as a mass separator and send purified ion bunches [35] to the two Penning traps: the preparation Penning trap which reduces the beam emittance further, and the precision Penning trap, where the ion mass is determined by the Time-of-Flight Ion-Cyclotron-Resonance (ToF-ICR) [36] or the Phase-Imaging Ion-Cyclotron-Resonance (PI-ICR) [37, 14] techniques.

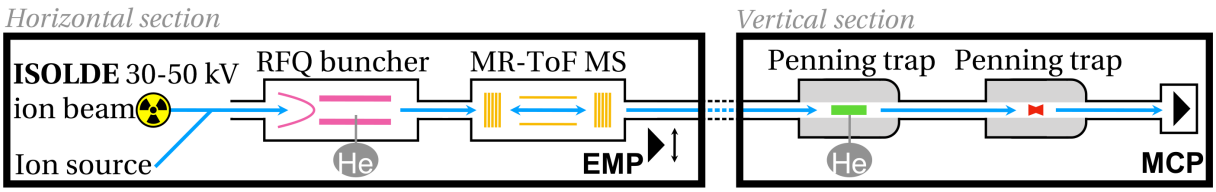

Figure 3: Schematic of the ISOLTRAP setup with its four ion traps and offline ion source.

Recently, the resolving power of the MR-ToF MS has been significantly improved to $> 4 \times 10^5$ by the implementation of a voltage stabilization system, which means that the MR-ToF MS can both measure nuclear states differing by about 500 keV (for an $A \approx 200$ ion) and more reliably eliminate contaminants, even in the presence of tails in the ToF peaks, with a $\approx 10^5$ resolving power.

Beam time request

We propose to produce the gold isotopes using a UC_x target (tantalum cavity) and resonant laser ionization. In table 1 we present the estimated yields and the requested shifts for the isotopes of interest. The estimation is based on values available in the ISOLDE yield database [38]: $4 \times 10^4/\mu$C for ^{201}Au and $1.4 \times 10^3/\mu$C for ^{202}Au. The release is based on production measurements from a UC_x target performed with the MR-ToF MS of ISOLTRAP and the Windmill decay station of KU Leuven in several experiments of in-source laser spectroscopy and mass measurements in the gold isotopic chain [39]. By using release model B (which gives the best description of the yields), we estimate a drop of a factor ≈ 2.5 between the in-target production of ^{201}Au and ^{202}Au. Taking this drop for all subsequent isotopes and twice its value as a worst-case scenario, we estimate for each isotope the yield range given in the table. These production rates are above the limits that ISOLTRAP can handle based on previous experiments (see for example [12, 40]). Expected surface ionized contamination will include thallium and francium. Thallium will be strongly suppressed due to its poor ionization in the tantalum transfer line. The francium contamination, however, will dominate on all mass numbers. To improve the

Table 1: Detailed beam request with isotope properties from [41] and estimated yields (see text for details). The spins marked with # are tentatively assigned.

Isotope	Half-Life	I^π	Yield [ions/μC]	Target / Ion source	Method	Shifts (8h)
$^{201-203}$Au	> 20 s	various	$> 10^3$	UC$_x$ / RILIS	MR-ToF MS/IDS	2
^{204}Au	38.3 s	2^-	110-440	UC$_x$ / RILIS	MR-ToF MS/PT	3
^{205}Au	32.0 s 6.0 s	$3/2^+$# $11/2^-$#	15-125	UC$_x$ / RILIS	MR-ToF MS/PT	4
^{206}Au	47.0 s	6^-#	5-110	UC$_x$ / RILIS	MR-ToF MS/PT	6
Beam optimization						2

contamination ratio, the line can be operated at a lower temperature and the ISOLDE beam gate can be synchronized to the proton pulses with a delay, in order to exploit the slower release of gold with respect to the much faster francium release.

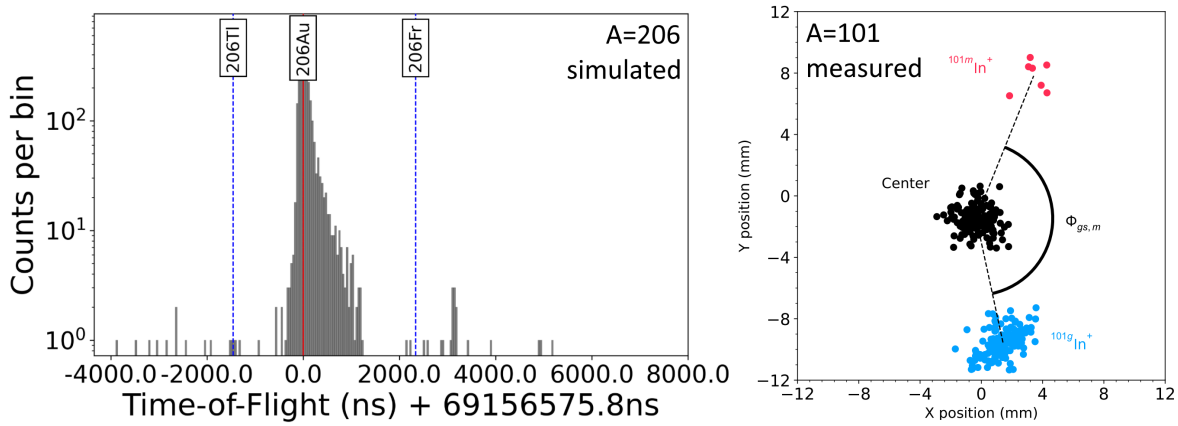

Figure 4: Left: Simulated ^{206}Au$^+$ bunch from the MR-TOF MS based on the present device performance, including expected positions of isobaric contaminants. Right: PI-ICR measurement of the ground and the 650 keV isomeric states of ^{101}In [42].

The remaining contamination will be cleaned by the ISOLTRAP purification methods, including the MR-TOF MS, the preparation Penning trap, and finally the measurement trap itself. The long half-lives of the gold isotopes allow to spend the necessary trapping time in order to achieve the maximum purification power of each ion trap. A simulated spectrum of ^{206}Au$^+$ with the expected positions of the isobaric contaminants is presented in fig. 4 (left), showing that the separation of ^{206}Fr$^+$ would be sufficient for MR-ToF MS purification, especially given that the gold peak is preceding the francium one, so it is not affected by the ToF peak tail. Two shifts are requested for optimizing stable beam and the purification method for each isotope. Another two shifts are requested for studying the beam composition and optimizing the target-ion-source parameters (including RILIS) on the less exotic isotopes. In this part of the experiment, the beam composition can also be studied using the highly sensitive ISOLDE decay station (IDS).
Summary of requested protons: 17 shifts in one run with a UC$_x$ target, and RILIS.

References

[1] O. Sorlin, M.-G. Porquet, *Progr. Part. Nucl. Phys.* **61**, 602 (2008).

[2] T. Otsuka, A. Gade, O. Sorlin, T. Suzuki, Y. Utsuno, *Rev. Mod. Phys.* **92**(1), 15002 (2020).

[3] C. Yuan, *et al.*, *Phys. Rev. C* **106**(4), 044314 (2022).

[4] M. Arnould, S. Goriely, K. Takahashi, *Phys. Rep.* **450**, 97 (2007).

[5] D. L. Fang, B. A. Brown, T. Suzuki, *Phys. Rev. C* **88**(3), 034304 (2013).

[6] B. Hu, *et al.*, *Nature Physics* **18**(10), 1196 (2022).

[7] T. Day Goodacre, *et al.*, *Phys. Rev. Lett.* **126**(3), 32502 (2021).

[8] M. Dworschak, *et al.*, *Phys. Rev. Lett.* **100**(7), 072501 (2008).

[9] R. N. Wolf, *et al.*, *Phys. Rev. Lett.* **110**, 41101 (2013).

[10] F. Wienholtz, *et al.*, *Nature* **498**, 346 (2013).

[11] M. Rosenbusch, others, *Phys. Rev. Lett.* **114**(20), 202501 (2015).

[12] A. Welker, *et al.*, *Phys. Rev. Lett.* **119**(19), 192502 (2017).

[13] D. Atanasov, *et al.*, *Phys. Rev. Lett* **115**(23), 232501 (2015).

[14] V. Manea, *et al.*, *Phys. Rev. Lett.* **124**(9), 092502 (2020).

[15] B. Jurado, *et al.*, *Phys. Lett. B* **649**(1), 43 (2007).

[16] A. Chaudhuri, *et al.*, *Phys. Rev. C* **88**(5), 54317 (2013).

[17] A. T. Gallant, *et al.*, *Phys. Rev. C* **96**(2), 024325 (2017).

[18] S. Michimasa, *et al.*, *Phys. Rev. Lett.* **121**(2), 022506 (2018).

[19] S. Iimura, *et al.*, *Phys. Rev. Lett.* **130**(1), 012501 (2023).

[20] M. Wang, W. J. Huang, F. G. Kondev, G. Audi, S. Naimi, *Chinese Phys. C* **45**(3), 030003 (2021).

[21] C. Izzo, *et al.*, *Phys. Rev. C* **103**(2), 25811 (2021).

[22] R. Taniuchi, *et al.*, *Nature* **569**(7754), 53 (2019).

[23] F. Nowacki, A. Poves, E. Caurier, B. Bounthong, *Phys. Rev. Lett.* **117**(1), 272501 (2016).

[24] P. Möller, A. J. Sierk, T. Ichikawa, H. Sagawa, *At Data Nucl. Data Tables* **109-110**, 1 (2016).

[25] S. Goriely, N. Chamel, J. M. Pearson, *Phys. Rev. C* **88**, 24308 (2013).

[26] M.-G. Porquet, O. Sorlin, *Phys. Rev. C* **85**(1), 14307 (2012).

[27] K.-H. Schmidt, D. Vermeulen, in *Atomic Masses and Fundamental Constants 6*, pp. 119–128. Springer US (1980).

[28] N. Zeldes, T. S. Dumitrescu, H. S. Köhler, *Nucl. Phys. A* **399**(1), 11 (1983).

[29] M. Bender, G. F. Bertsch, P.-H. Heenen, *Phys. Rev. C* **73**, 34322 (2006).

[30] V. Manea, M. Mougeot, D. Lunney, *Eur. Phys. J. A* (submitted 2022).

[31] S. Goriely, *et al.*, *Phys. Rev. Lett.* **111**, 242502 (2013).

[32] M. Mukherjee, *et al.*, *Eur. Phys. J. A* **35**(1), 1 (2008).

[33] R. N. Wolf, *et al.*, *Int. J. Mass Spectrom.* **349–350**(0), 123 (2013).

[34] F. Herfurth, *et al.*, *Nucl. Instr. Meth. A* **469**(2), 254 (2001).

[35] F. Wienholtz, S. Kreim, M. Rosenbusch, L. Schweikhard, R. N. Wolf, *Int. Journ. Mass Spectrom.* **421**, 285 (2017).

[36] M. König, G. Bollen, H.-J. Kluge, T. Otto, J. Szerypo, *Int. J. Mass Spectrom.* **142**, 95 (1995).

[37] S. Eliseev, *et al.*, *Phys. Rev. Lett.* **110**(8), 082501 (2013).

[38] T. Stora, *Nucl. Instr. Meth. B* **317**, 402 (2013).

[39] A. E. Barzakh, *et al.*, *Nucl. Instr. Meth. B* **513**, 26 (2022).

[40] M. Mougeot, *et al.*, *Phys. Rev. Lett.* **120**(23) (2018).

[41] W. Huang, M. Wang, F. Kondev, G. Audi, S. Naimi, *Chinese Phys. C* **45**(3), 030002 (2021).

[42] M. Mougeot, *et al.*, *Nature Phys.* **17**, 1099 (2021).

DESCRIPTION OF THE PROPOSED EXPERIMENT

The experimental setup comprises: ISOLDE central beam line and ISOLTRAP setup. For two of the shfits, the ISOLDE Decay Station could be used (see table 1). The ISOLTRAP setup has safety clearance, the memorandum document 1242456 ver.1 "Safety clearance for the operation of the ISOLTRAP experiment" by HSE Unit is released and can be found via the following link: `https://edms.cern.ch/document/1242456/1`.

Part of the	Availability	Design and manufacturing
ISOLTRAP setup	☒ Existing	☒ To be used without any modification
IDS setup	☒ Existing	☒ To be used without any modification

HAZARDS GENERATED BY THE EXPERIMENT

Hazards are named in the document relevant for the fixed ISOLTRAP installation.